heritage

MDPI

Article

A Semi-Automated Machine-Learning Tool for Assessing Building Phases: Discriminant Analysis of Mortars from the 2022 Excavation at the Sarno Bath Complex in Pompeii

Simone Dilaria [1,2,*], Caterina Previato [1,*], Michele Secco [1,2] and Maria Stella Busana [1]

[1] Department of Cultural Heritage: Archaeology, History of Art, Cinema and Music (DBC), University of Padua, Piazza Capitaniato 7, 35139 Padua, Italy; michele.secco@unipd.it (M.S.); mariastella.busana@unipd.it (M.S.B.)
[2] Inter-Departmental Research Centre for the Study of Cement Materials and Hydraulic Binders (CIRCe), University of Padua, Via Giovanni Gradenigo 6, 35131 Padua, Italy
* Correspondence: simone.dilaria@unipd.it (S.D.); caterina.previato@unipd.it (C.P.)

Abstract: This study presents the results of the analyses of 15 structural mortars from the building at civ. 21, level +0 of the Sarno Bath complex in Pompeii. These samples were collected during recent stratigraphic excavations (year 2022) for detailed in-laboratory compositional characterization, aiming to trace the construction phases of the originating walls. The 2022 samples were firstly analyzed via quantitative phase analysis–X-ray powder diffraction. The resulting quantitative mineralogical profiles were then processed alongside those analyzed in previous studies from level +0 structures of the Sarno Baths using multivariate statistical methods, including principal component analysis (PCA) and discriminant analysis, applied to quantitative phase analysis (QPA)–X-ray powder diffraction data (XRPD), to identify and map the construction phases. This approach enabled the correlation of the 2022 samples with previously established construction phases. Polarized-light optical microscopy and scanning electron microscopy (SEM) coupled with energy dispersive X-ray spectroscopy (EDS) were then primarily used for validation purposes. These methods highlighted the compositional differences between samples and revealed significant features related to the use of specific raw materials. These results confirm the reliability of the semi-automated sample processing proposed in this research, adopting discriminant analysis as a machine-learning-based tool for defining construction phases in Pompeian contexts.

Keywords: ancient mortars; QPA-XRPD; discriminant analysis; principal component analysis; Somma–Vesuvius; Phlegraean Fields

Academic Editor: João Pedro Veiga

Received: 23 December 2024
Revised: 12 January 2025
Accepted: 21 January 2025
Published: 27 January 2025

Citation: Dilaria, S.; Previato, C.; Secco, M.; Busana, M.S. A Semi-Automated Machine-Learning Tool for Assessing Building Phases: Discriminant Analysis of Mortars from the 2022 Excavation at the Sarno Bath Complex in Pompeii. *Heritage* **2025**, *8*, 51. https://doi.org/10.3390/heritage8020051

1. Introduction

Archaeometric research on ancient mortars, investigated by adopting a diverse array of analytical techniques, has become increasingly common in the last decade. The selection of analytical methods is guided by the research objectives and the study's context. At Pompeii, mortar analyses have often been employed to examine compositional characteristics from a diachronic perspective or in relation to their functional application. A central aim in the compositional analysis of Vesuvian mortars has been to emphasize petrographic and mineralogical variations, facilitating the identification and chronological sequencing of construction phases in specific buildings. These tasks were usually achieved by adopting traditional approaches, primarily based on polarized-light optical microscopy investigations [1–4]. Other studies have combined multiple analytical techniques to distinguish mortars by their production chronology and corresponding construction phases, leveraging specific petrographic, mineralogical,

and geochemical variations [5–8]. Recently, the complex building history of the Sarno Bath complex, studied by researchers from the University of Padua, has offered a unique opportunity to investigate a lesser-known building at Pompeii. The construction phases of this building had remained uncertain due to the absence of detailed modern excavation reports and archival documentation from early-20th-century restorations. Therefore, mortar analysis has been used to distinguish the construction phases of the building by examining their compositional characteristics. Secco et al. [9] and Dilaria et al. [10] centered their analyses on a mineralogical characterization approach utilizing QPA-XRPD, which identified consistent mineralogical assemblages indicative of building phase sequences. These mineralogical assemblages were properly framed by processing via PCA (principal component analysis) of the QPA-XRPD data, which successfully differentiated mortar groups according to reliable ancient and modern construction and restoration phases. By characterizing mortar groups aligned with the building phases of the complex, this approach offers valuable insights into the construction history of the Sarno Baths.

The current research builds upon previous studies and aims to analyze a new dataset of mortar samples collected during stratigraphic excavations at the house located at civ. 21 (level +0) of the Sarno Bath complex (*Regio* VIII, *Insula* 2, n. 17–21) (Figure 1a,b).

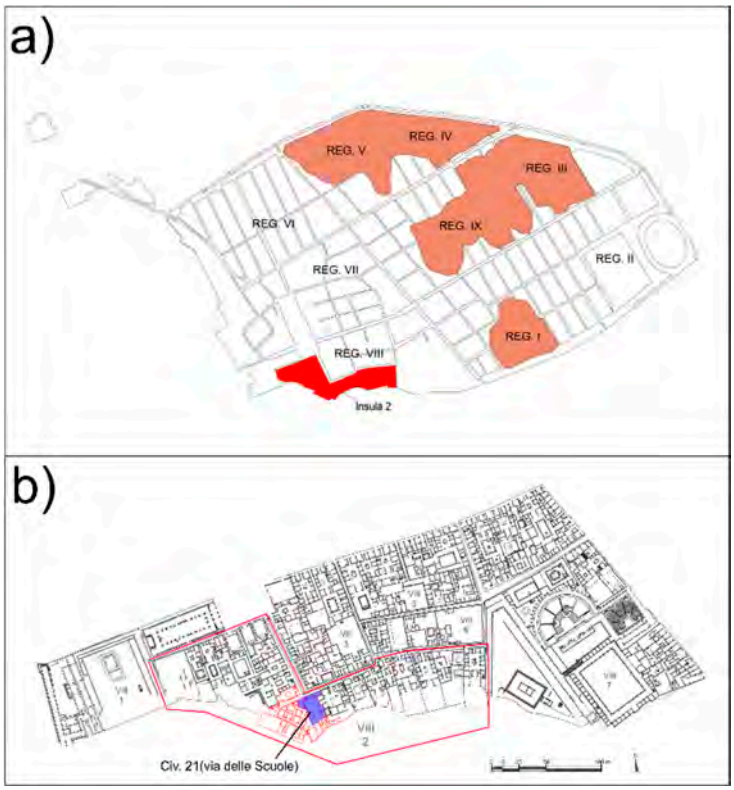

Figure 1. (**a**) General plan of Pompeii with indication of *Insula* 2 in *Regio* VIII; (**b**) Indication of the house at civ. 21 in Via delle Scuole, within the Sarno Bath Complex (modified from [10]).

The recent excavations, conducted in 2022 by the Department of Cultural Heritage at the University of Padua, were carried out in collaboration with the Archaeological Park of Pompeii, under the scientific coordination of M.S. Busana. The samples were initially analyzed using QPA-XRPD, and their mineralogical quantitative profiles were integrated into the existing dataset of previously analyzed mortar samples from the Sarno Bath complex. The statistical distribution of the new samples was then compared with the existing data, revealing overlaps within distribution clusters. However, certain samples presented uncertainties that could not be fully addressed by PCA.

To further validate these observations and enhance the attribution of samples to specific construction phases, a discriminant analysis (DA) approach was adopted. This multivariate statistical method, often used for predictive purposes [11], classifies data into categories based on posterior probabilities calculated from observed features. Using a training dataset with pre-classified samples as markers, DA estimates the likelihood that new observations belong to a specific category by considering variable distributions and prior probabilities. In essence, DA compares the position of data points relative to the centers of class distributions while accounting for internal variability, assigning samples to categories that have the highest posterior probability. In archaeology, DA has been applied to relate new observations to classified datasets, particularly in probabilistic determinations comparing archaeological geomaterials (e.g., stone, ceramics) with geologically compatible samples from known sources [12–16]. In this study, DA was innovatively employed as a machine-learning tool for automated phase attribution, based on the compositional compatibility of mortar samples from the 2022 excavation with those previously analyzed and linked to known construction phases. Pre-classified samples from level +0, analyzed in [10], served as training markers. By analyzing the mineralogical affinities of samples, DA assigned the unknown-phase 2022 samples to specific construction phases based on their probabilistic compatibility with known-phase samples, using two confidence intervals.

Both PCA and DA analysis were developed using multivariate statistical tools integrated into Statgraphics Centurion PRO 19 (© 2023 Statgraphics Technologies, Inc., The Plains, VA, USA). The data were ultimately validated through cross-comparison with optical microscopy analysis of samples prepared as 30 µm thin sections. Additionally, SEM-EDS analyses provided insights into the potential sources of the volcanic aggregate fraction further validating the mineralogical differences observed after QPA-XRPD analyses and PCA/DA associations. These findings enhanced the chronological framework of the construction phases and corroborated stratigraphic hypotheses established through field archaeological investigations.

2. The Previous Research

Research on the Sarno Bath complex in Pompeii began in 2016, focusing on a multianalytical examination of its construction history and state of preservation. This included investigating construction techniques, seismic monitoring, archival data on the building's history, and the materials used, including structural mortars [17].

The Sarno Bath complex, situated in *Regio* VIII, *Insula* 2 near the Forum, represents a significant Roman spa complex constructed on Pompeii's southwestern volcanic plateau [18]. Initially excavated between 1887 and 1890, with additional façade work in the 1950s, the site has a long history of use, dating back to the Archaic and Samnite periods. By the 2nd century BCE, during the Late Republican period, terraced *domus* were built in this area. The baths were realized in a later period and, in their final arrangement, spanned approximately 3700 m^2 across four terraced floors descending the plateau, featuring a façade with an entrance overlooking the Sarno Valley. The ground floor (level +0) comprised three interconnected housing units with independent entrances, today accessible from Vicolo della Regina and Via delle Scuole. Below, level -1 housed cisterns and service rooms were accessed via a vaulted corridor. Level -2 contained three panoramic apartments connected by a decorated cryptoporticus, while level -3 housed the actual baths and seven small rooms of uncertain function along a windowed corridor. Finally, level -4 included five service rooms, above a thick *opus caementicium* foundation.

The multidisciplinary research conducted by the University of Padua provided a deeper understanding of the complex's construction history, enabling the identification of four key phases of its construction and restoration [19].

- Phase I: Isolated structures with unspecified function and chronology identified underneath later buildings of phase II.

- Phase II: Construction of at least two terraced *domus*, including walls and floors and equipped with water cisterns, certainly before the Imperial age.
- Phase III: Reorganization of the *domus* into their current layout likely occurred after the Augustan age (early 1st century CE). This phase involved reframing earlier structures and filling pits that remained incomplete at the time of the 79 CE eruption. A large terraced building was constructed during this phase, housing (or intended to house) the thermal baths on levels -3 and -4, accessible independently via a tunnel leading to Vicolo della Regina.
- Phase IV: 19th- and 20th-century restorations, often poorly documented, altered the original layout and plan of the buildings.

A crucial contribution to the identification of the construction phases came from the analyses of structural mortar samples discussed in [9,10]. Overall, around 80 mortar samples from both dated and undated structures were analyzed using optical microscopy (OM) and X-ray powder diffraction with quantitative phase analysis (QPA-XRPD). Principal component analysis (PCA) of the QPA-XRPD data classified the samples into three main groups, aligned with distinct construction phases and restoration periods. OM validated these groupings by confirming the statistical differentiation of the mineralogical profiles. The groupings attributions are reported hereafter.

- ➢ Group 1: Modern restoration mortars (phase IV), subdivided into Gr 1a, 1b, and 1c, corresponding to specific restoration interventions. Gr 1c mortars likely date to 19th-century restorations, as supported by thermoluminescence dating of bricks [9]. Gr 1b mortars, characterized by leucite-rich materials, suggest restorations postdating the 1930s.
- ➢ Group 2: Mortars dated between the end of the Augustan age and 79 CE (phase III), with subgroups Gr 2a and 2b. These likely reflect construction activities before and after the earthquake of 62/63 CE.
- ➢ Group 3: Mortars attributed to two sub-groups. Subgroup Gr 3a aligns with structures dated to the pre-Imperial age (phase I–II), while for 3b the chronological association is unclear.

PCA analysis identified distinct mineralogical markers differentiating the phases, as reported below. These findings, combined with stratigraphic and archival data, provide a robust chronological framework for understanding the Sarno Baths' architectural evolution before and after the 79 CE eruption of Mt. Vesuvius.

3. The 2022 Excavations at Civ. 21

During the 2022 campaign two excavation trenches were opened at the ground floor (level +0) of the house at civ. 21 of Via delle Scuole. The first one was located in correspondence with rooms G1 and G2 (sector D) and the second one in correspondence with room O (sector E). In both sectors, the excavation activity brought to light structures attributable to the two already known building phases of the complex, namely phase II (pre-Imperial age) and phase III (post-Augustan age). In particular, in sector D it was possible to distinguish some structures and layers certainly belonging to the house currently visible at civ. 21 (phase III) and structures and floors attributable to the earlier building already partially investigated in 2018–2019, called 'Casa A' (phase II). A similar situation was observed in sector E, where both structures related to the *domus* currently visible at civ. 21 (phase III) and evidence referring to a pre-existing *domus* (the so-called 'Casa B', phase) were found.

Regarding chronology, the 2022 excavation finds suggest that the *domus* at civ. 21 was constructed during the 1st century CE and the work was still in progress in 79 CE, while the earlier *domus* (Casa A and Casa B) were likely built in the second half or towards the end of the 2nd century BCE or at the beginning of the 1st century BCE.

4. The 2022 Sampling

In the 2022 research campaign, 15 lime mortar samples were taken and analyzed (Figure 2). They all consisted of bedding mortars of masonry structures (Table 1). Among the wall structures sampled, some were attributed, on a stratigraphic basis, to a specific building phase. This is the case, for example, of walls USM 304 and 302, referable to the so-called 'Casa A' (phase II), and walls USM 81 and 83, clearly part of the more recent *domus* at civ. 21 (phase III). For other structures, the archaeological stratigraphic sequence did not provide clues to identify a possible construction phase. In particular, in some cases, it was unclear whether the entire structure belonged to the same construction phase or if the upper elevation was more recent, built on an older foundation. This is the case, for instance, for walls USM 80, 300, and 301. Given this uncertainty, a sample was taken from both the foundation and the elevation of each structure.

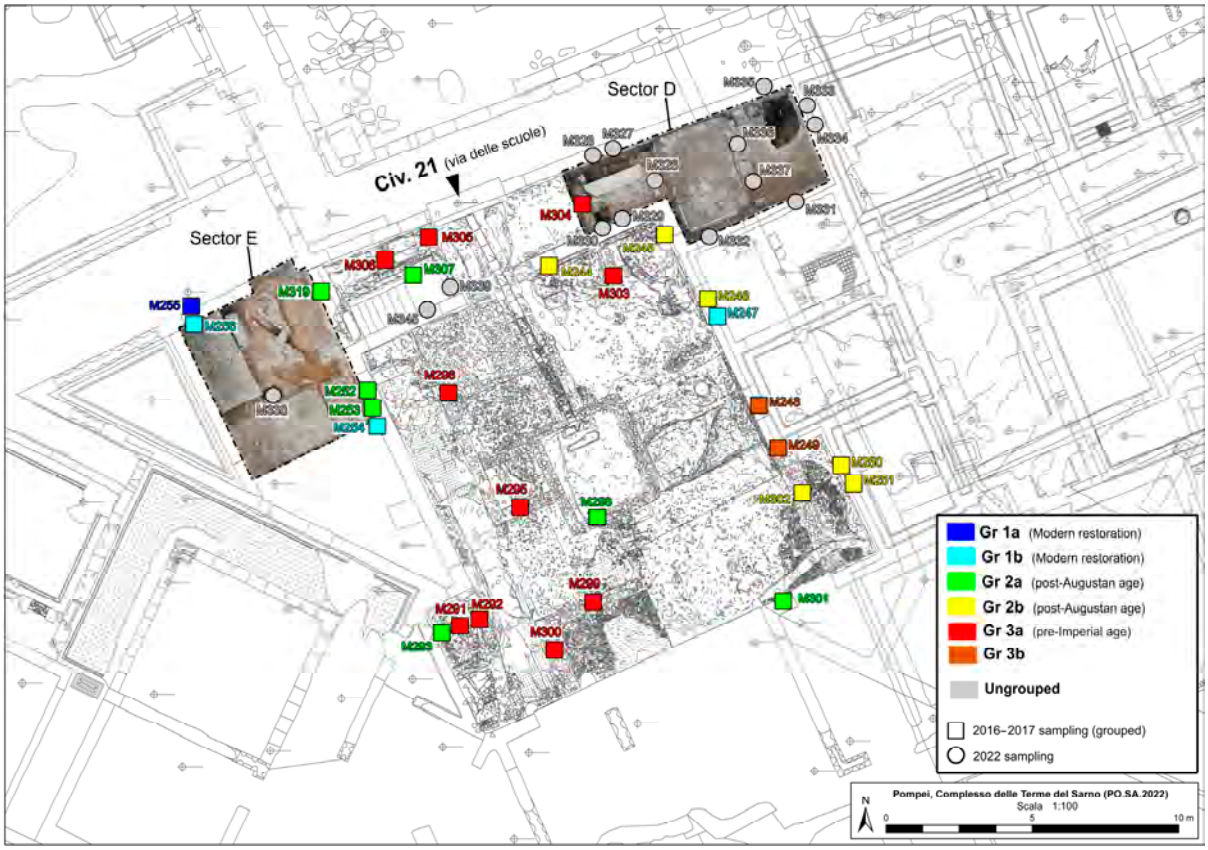

Figure 2. Samples collected from the 2022 excavation (circular labels in grey) together with those already analyzed from civ. 21 and associated to groups identified in [10].

With regard to the construction techniques of the sampled walls, no particular differences were observed. In fact, the foundations all consist of irregular stone elements bonded by lime mortar and arranged in an irregular manner (*opus incertum*). Different lithotypes are often used within the same structure; however, in most cases, compact and vesicular tephrite are most prevalent as masonry elements (Figure 3a). Regarding the elevated portions, two distinct techniques were identified. The first technique involves the use of irregular stone elements of various lithologies (predominantly travertine), arranged in an irregular pattern (*opus incertum*) and bound with lime mortar (Figure 3b). The second technique involves the exclusive use of yellow tuff, shaped into sub-rhomboidal elements arranged in rows, inclined at a 45-degree angle (*opus quasi reticulatum*) (Figure 3c).

Table 1. Samples collected from the 2022 excavation with indication of the structural function, materials, construction technique, and hypothetical building phase (attributed on a stratigraphic basis) of the wall structures sampled.

Sample	Wall Number	Structural Function	Building Materials	Building Technique	Hypothetical Building Phase (Based on Archaeological Data)
M326	USM338	Foundation	Compact and vesicular tephrite	*Opus incertum*	II
M327	USM83	Foundation	Vesicular tephrite, yellow tuff, travertine	*Opus incertum*	III
M328	USM83	Elevation	Yellow tuff	*Opus quasi reticulatum*	III
M329	USM81	Foundation	Compact tephrite	*Opus incertum*	Not determined
M330	USM81	Elevation	Yellow tuff + bricks (in the chains)	*Opus quasi reticulatum*	III
M331	USM301	Foundation	Compact tephrite	*Opus incertum*	Not determined
M332	USM301	Elevation	Yellow tuff	*Opus quasi reticulatum*	III
M333	USM300	Foundation	Vesicular tephrite, white limestone, travertine, bricks	*Opus incertum*	Not determined
M334	USM300	Elevation	Travertine, compact and vesicular tephrite, grey tuff	*Opus incertum*	III?
M335	USM83	Foundation	Vesicular tephrite, yellow tuff, travertine	*Opus incertum*	Not determined
M336	USM304	Foundation	Compact and vesicular tephrite, travertine, bricks	*Opus incertum*	Not determined
M337	USM304	Foundation/ Threshold basis?	Compact and vesicular tephrite, travertine, bricks	*Opus incertum*	Not determined
M338	USM515	Foundation	Travertine	*Opus incertum*	Not determined
M339	USM 173	Elevation	Compact tephrite, reused brick fragments	*Opus incertum*	Not determined
M345	n.d.	Elevation, corner chain	Grey tuff, bricks	*Opus vittatum mixtum*	Not determined

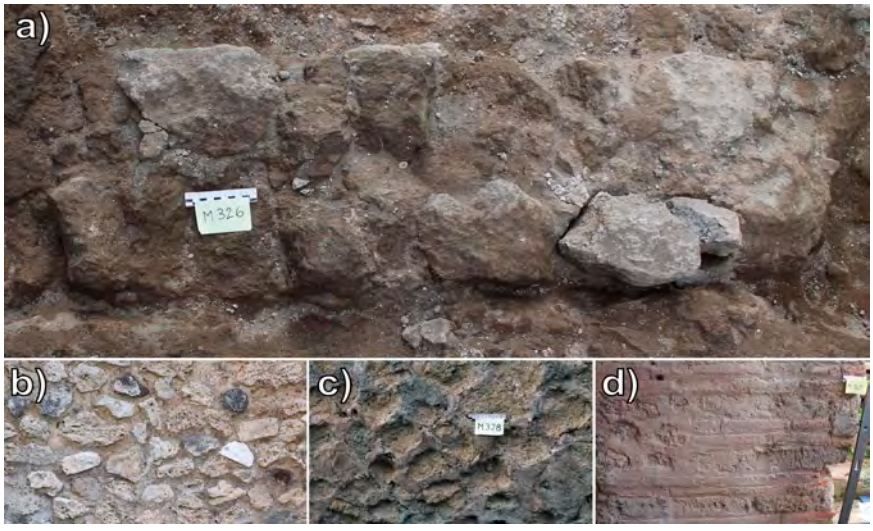

Figure 3. The building techniques used in the wall structures sampled: (**a**) foundation in *opus incertum*; (**b**) elevation in *opus incertum*; (**c**) elevation in *opus quasi reticulatum*; (**d**) elevation in *opus incertum*.

Typically, bricks are used to construct the corner chains in this type of structure. Another documented technique is *opus vittatum mixtum* (Figure 3d), seen in the corner chain of the west wall of the tunnel leading to the lower floor. This technique consists of alternating courses of parallelepiped blocks of grey tuff and bricks.

5. Analytical Workflow and Data Processing

From an analytical perspective, all samples were initially analyzed using QPA-XRPD (see Supplementary Materials S1 for instrumental parameters and equipment details [16,20–22]) to facilitate a mineralogical comparison with the samples reported in [9,10]. Beyond identifying the primary mineral phases in the mortar samples (Figure 4), XRPD analysis also clearly revealed secondary phases associated with alteration processes in some mortars from already exposed structures (raised walls). These included gypsum, halite, and gaylussite, which were linked to the migration and crystallization of soluble salts, as described in [23]. In particular, gypsum was identified as a product of atmospheric weathering on exposed mortars, consistent with previous studies [5,24]. Halite, another common alteration product in ancient mortars, was similarly detected [25]. To ensure consistency in the analysis, the proportions of the remaining primary mineral phases were recalculated to 100% wt (see Supplementary Materials S2).

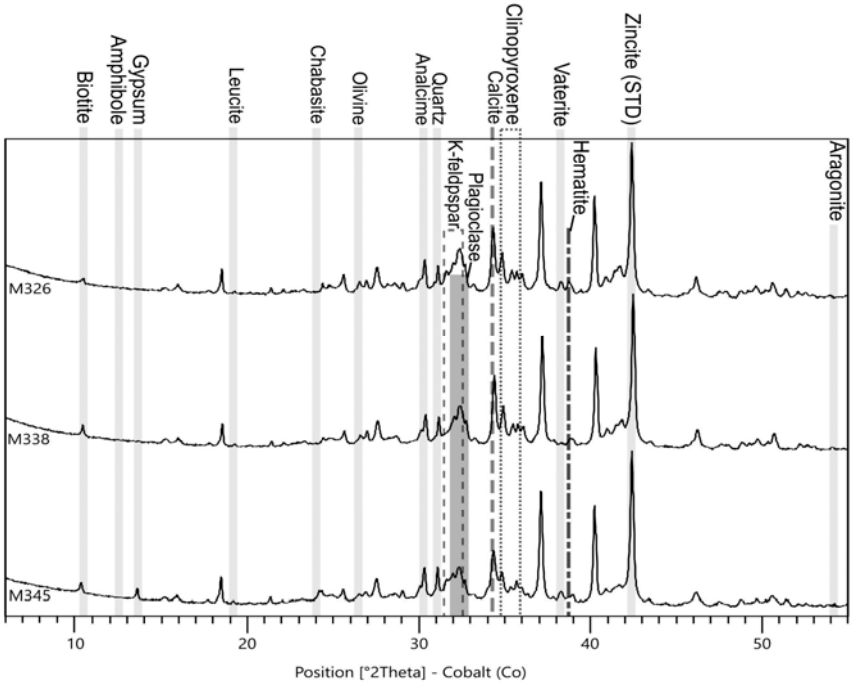

Figure 4. XRPD spectra of representative mortar samples from the 2022 excavation, showing the d-spacing of the principal peak of all mineral phases other than amorphous. For those mineral phases overlapping their main peaks, an indicative secondary peak has been highlighted (i.e., aragonite).

5.1. PCA on Mineralogical Data

The resulting mineralogical data were reprocessed alongside the samples analyzed in [10] from level +0 of the Sarno Baths using PCA. This statistical method extracts a limited number of linear combinations that effectively capture the variability of the original mortar mineralogical profiles. It generates a set of principal components that represent the dataset's variations. This analysis employed the original mineralogical phases of the mortar samples as descriptive variables (recalculated at 100%wt after the removal of the alteration phases). The sample distribution was reported in a scatterplot according to the value of the first two extracted components (PC1, PC2), as the first two components are those describing the main variance of the dataset. The resulting bivariate diagram (Figure 5) highlights strong correlations between the 2022 excavation samples and the previously analyzed samples.

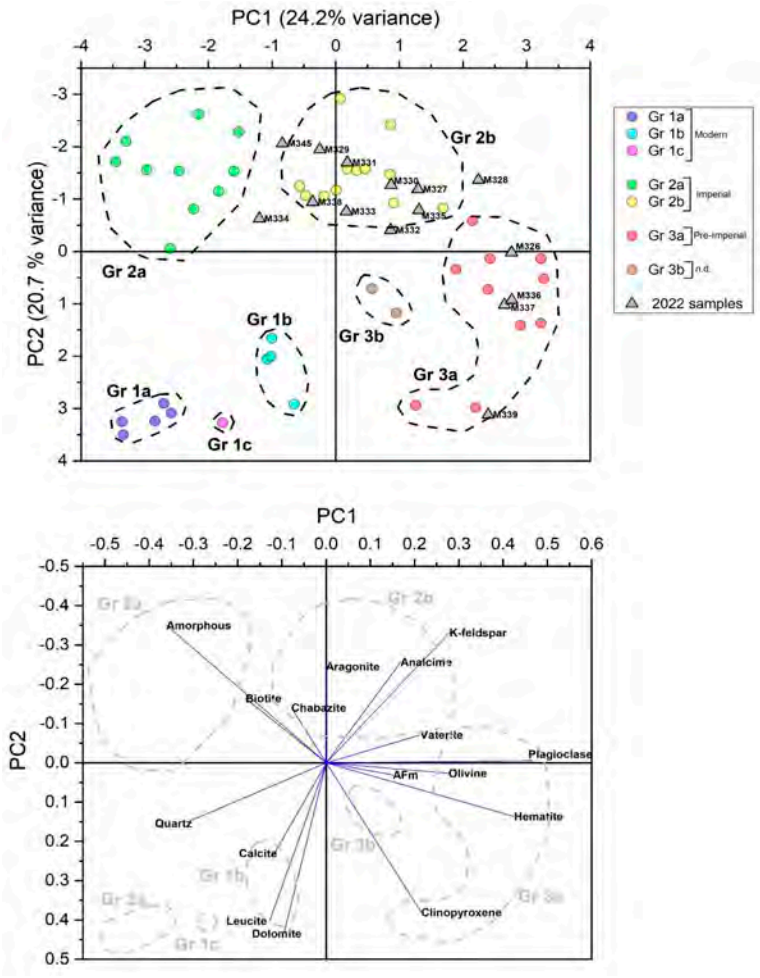

Figure 5. PCA distribution of the 2022 excavation samples according to QPA-XRPD data (triangles), processed together with mortar from level +0, in colored dots according to final groupings identified in [10].

The PCA distribution diagram shows a trend in the PC1 and PC2 axes similar to that observed in [10], with vectors indicating mineralogical phases that are interrelated and characteristic of the identified sample groups:

- Group 3a (PC1 and PC2 values between 0 and +4). This group comprises samples attributed to the pre-Imperial construction period. The connoting mineral phases, positively correlated with group distribution, include hematite, plagioclase, olivine, and, subordinately, clinopyroxene (Cpx). Some 2022 samples, such as M339, M336, M337, and M326, fall within this range.
- Group 3b (PC1 and PC2 ~+1). No 2022 excavation samples clearly align with this subgroup.
- Group 2a (PC1: −1 to −4, PC2: 0 to −3). These samples, dating to the pre-79 CE Imperial phase, are characterized by high concentrations of amorphous phases and biotite. None of the 2022 samples fall directly within this interval. However, samples M334 and M345 lie in intermediate positions between groups 2a and 2b.
- Group 2b (PC1: −1 to +2, PC2: 0 to −3): This group also collects samples from the pre-79 CE Imperial phase. This group is defined by positively correlated phases such as K-feldspar, analcime, and, to a lesser extent, aragonite. Most 2022 samples, including M327, M329, M330, M331, M333, M335, and M338, and, align with this group. Petrographic analysis reveals a higher concentration of pyroxenes (augite), olivine, and volcanic clasts with K-feldspar microlites (sanidine) compared to group 2a mortars.

- Modern restoration mortars (groups 1a, 1b, and 1c, PC1: 0 to −4, PC2: 0 to +4): These groups are defined by positive correlations with calcite, leucite, dolomite, and quartz. None of the 2022 samples fall within or near this quadrant, suggesting no modern restoration mortars were sampled.

From the PCA results, even if it is clear that no 2022 samples correspond to modern restoration mortars, certain correlations between some samples and specific groups remain ambiguous. In fact, several samples occupy intermediate positions, particularly between groups 3a and 2a/2b. This suggests that, while the 2022 samples align with established construction phases, mineralogical fingerprints alone may not definitively associate samples with specific groups. This is partly due to the inherent limitations of PCA analysis, as the first two PCs together account for only about 45% of the total dataset's variability. Secondary correlations can be explained by analyzing the remaining PCs with eigenvalues greater than or equal to 1.0 (PC3 to 6), which, however, account for minor fractions of the dataset's variability (each contributing less than 10%).

5.2. Discriminant Analysis of Mineralogical Data

Discriminant analysis was employed as a machine-learning predictive method to automatically attribute samples of uncertain phase to a specific construction phase. The training dataset comprised the same samples used in the PCA analysis, representing structures already assigned to construction phases of level +0 of the Sarno Bath complex. Mineralogical phases descriptive of the dataset served as independent discriminant variables, while the 2022 excavation samples were treated as uncertain data to be probabilistically associated with a construction phase based on their compatibility with the centroids of the reference sample groups. A total of 45 cases were used to develop a model to discriminate among the six levels of attribution. Using a stepwise selection algorithm, it was determined that six variables (amorphous, analcime, hematite, olivine, leucite, dolomite) were significant predictors of group. The four discriminating functions with p-values less than 0.05 are statistically significant at the 95.0% confidence level. The data processing enabled the assignment of most samples to a specific group (i.e., construction phase) with high confidence (>99% for 1st probability), as reported in Table 2.

Table 2. Results of the discriminant analysis (DA, stepwise method—forward selection) on the samples from the 2022 excavation attributed to groups at two probabilistic intervals.

Sample	Assigned Group (1st)	Prob. (%)	Assigned Group (2nd)	Prob. (%)	Based on PCA
M326	3a	100	*null*	*null*	3a
M336	3a	100	*null*	*null*	3a
M337	3a	100	*null*	*null*	3a
M339	3a	100	*null*	*null*	3a
M327	2b	100	*null*	*null*	2b
M328	2b	100	*null*	*null*	2b ?
M329	2b	99.87	2a	0.13	2b
M330	2b	99.03	3b	0.97	2b
M331	2b	99.98	2a	0.02	2b
M333	2b	99.98	3b	0.02	2b
M334	2b	99.41	2a	0.59	2a or 2b
M335	2b	100	*null*	*null*	2b
M338	2b	99.06	2a	0.94	2b
M345	2a	88.37	2b	11.63	2a or 2b
M332	3b	51.85	2b	48.15	2b ?

- Group 3a: Samples M326, M336, M337, and M339 were confidently assigned to this group, consistent with the PCA results.
- Group 2b: Samples M327, M328, M329, M330, M331, M333, M334, M335, and M338 were reliably attributed to this group.
- Group 2a: Sample M345 was assigned to group 2a with good probability (88.37% 1st probability); however, a potential association with group 2b cannot be excluded (11.63% 2nd probability), highlighting the difficulty in definitively attributing this sample to one of these groups.
- Sample M332: This sample's attribution remains uncertain. DA indicated nearly equal probabilities of belonging to group 3b or group 2b. This uncertainty is possibly due to the limited representativeness of the reference dataset, which lacks the larger, categorized markers (e.g., phased mortars) typically used in DA. Expanding the dataset with more reference markers could significantly reduce this uncertainty. Based on PCA observations of the first two principal components, this sample seems more compatible with group 2b.

5.3. OM and SEM-EDS Analyses (Data Verification)

The results of the statistical processing of the mineralogical descriptive data were subsequently validated through petrographic and chemical characterization of the compounds, using transmitted light optical microscopy and SEM-EDS investigations of representative samples prepared in 30 μm thin sections (see Supplementary Materials S1 for details on instrumental parameters and equipment [16,20–22]) This analysis further confirmed the attribution of the samples based on the distinctive petro-mineralogical features that characterize the mortars sampled in the 2022 archaeological campaign. The samples attributed to group 3a (M326, M336, M337, and M339) are primarily composed of highly vesicular tephrites exhibiting a hypocrystalline hyalopilitic structure. These aggregates contain scattered phenocrysts, typically constituted by clinopyroxenes (augite–diopside) and feldspars, predominantly of the plagioclase variety (labradorite/bytownite), with subordinate K-feldspars (sanidine), often arranged as glomerophyres (Figure 6a). Moreover, single-grained leucite phenocrysts are usually almost completely transformed into analcime due to analcimization processes [26] (Figure 7(a–b2)). Accessory minerals include olivine, biotite, hematite, and opaque minerals (Figure 8(a1–a3)). The vesicular tephrite component ranges from multi-millimeter-sized clasts to powdered fractions, forming cineritic shards tightly blended with the lime-based binder. The binder is carbonate-based, homogeneous, micritic, and thoroughly integrated with such scoriaceous aggregate, typically in binder-to-aggregate (B:A) ratios of approximately 1:2 or 1:3. Unmixed lime lumps are minimal. The mortar porosity is low, with rounded vesicle-type pores predominating. A completely subordinate fraction of the aggregate is constituted by extremely scattered grains of pyroclastic rocks (pumices).

The samples confidently attributed to group 2b (M327, M328, M329, M330, M331, M333, M334, M335, and M338) include the same highly vesicular tephrites found in group 3a (Figure 6b). However, in the mortars of group 2b, these tephrites are mixed in comparable proportions with pumice clasts exhibiting reacted borders. They can be classified into two main types: one is highly vesicular and aphyric/vitrophyric, with scattered biotite phenocrysts (Figure 8(b1–b3)), while the other is feebly porphyritic/hyalopilitic with reduced internal vascularity (Figure 8(c1–c3)). Rarely, scattered tuffs with cineritic matrices were identified. They embed pumices, volcanic shards, and individual mineral components such as biotite, K-feldspar, occasional clinopyroxenes, and opaque minerals. A subordinate component of the aggregate includes grains of effusive rocks with porphyritic/trachytic textures, characterized by feldspars with sanidine > plagioclase > anorthoclase, and opaque

minerals, along with accessory clinopyroxenes and biotite. The carbonate binder in these samples is micritic to microsparitic, slightly heterogeneous, with a greater occurrence of poorly mixed lime lumps. The binder-to-aggregate ratio (L:A) tends towards 1:2. The open porosity is scarce and primarily constituted by vugh/vesicle type voids.

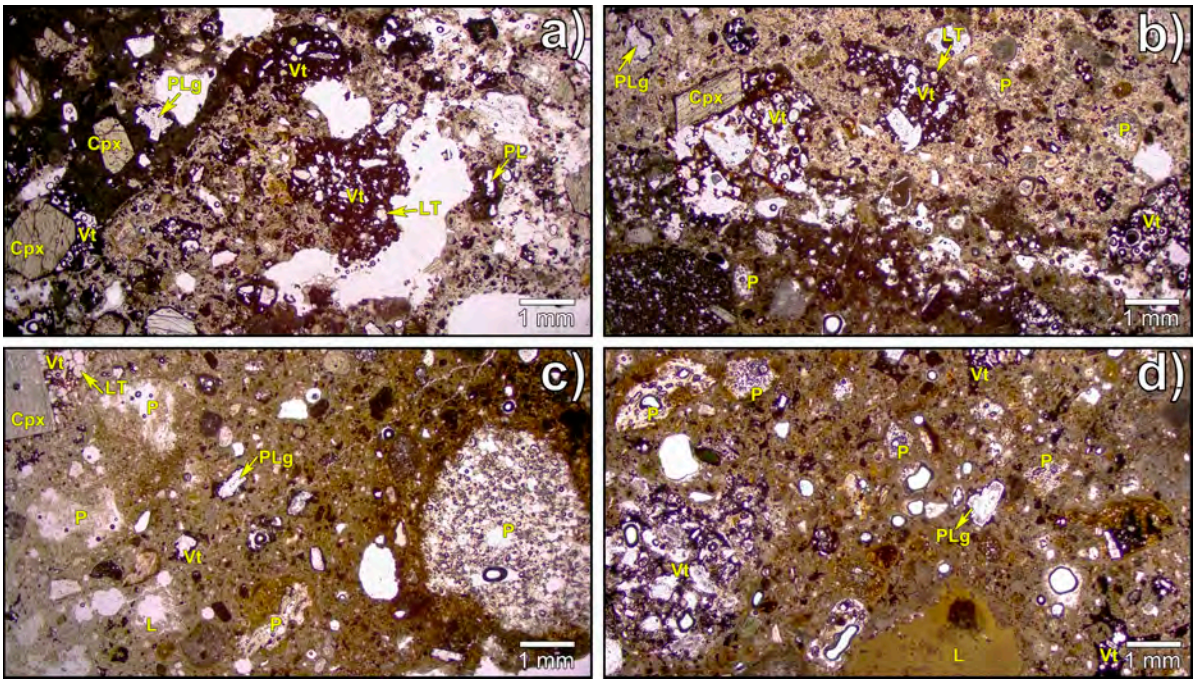

Figure 6. Micrographs in optical microscopy with transmitted polarized light (parallel nicol) of representative samples from the groups previously defined. (**a**) M326 (group 3a); (**b**) M338 (group 2b); (**c**) M345 (group 2a); (**d**) M332 (compatible with group 2b). Legend: Vt = vesicular tephrite; *p* = pumice; PL = plagioclase; PLg = plagioclase (glomerophyre); L = lump; LT = leucite (usually analcimized); Cpx = clinopyroxene.

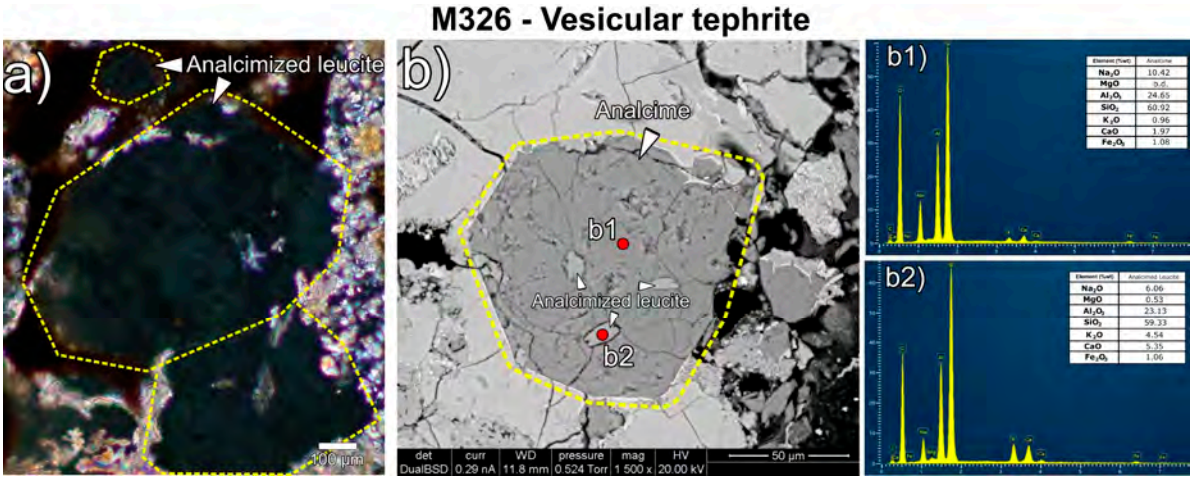

Figure 7. Analcimized leucite mineralization in a vesicular tephrite clast included in sample M326. (**a**) TL-OM cross-polar high-magnification micrograph of analcimized leucite. (**b**) SEM image (backscattered electron) of the analcimized leucite; (**b1**,**b2**) EDS microanalyses in two points of the analcimized leucite.

Sample M345 differs from the group 2b samples as its aggregate fraction is primarily composed of aphyric juveniles with scattered biotite phenocrysts, and slightly porphyritic/hyalopilitic pumices. The presence of grains and shards of vesicular tephrite

(Figure 6c) is significantly lower. Based on these characteristics, it may be classified with the group 2a mortars, which are connoted by a high concentration of amorphous material and biotite, quantified also after QPA-XRPD analyses, indicative of the elevated pumice fraction included in the sample constituting this group. A totally subordinate component of the aggregates consists of more compact tephrite grains. These grains often contain phenocrysts of biotite, clinopyroxene, plagioclase, and minerals of leucite, with a lower degree of analcimization (Figure 9(a–a2)).

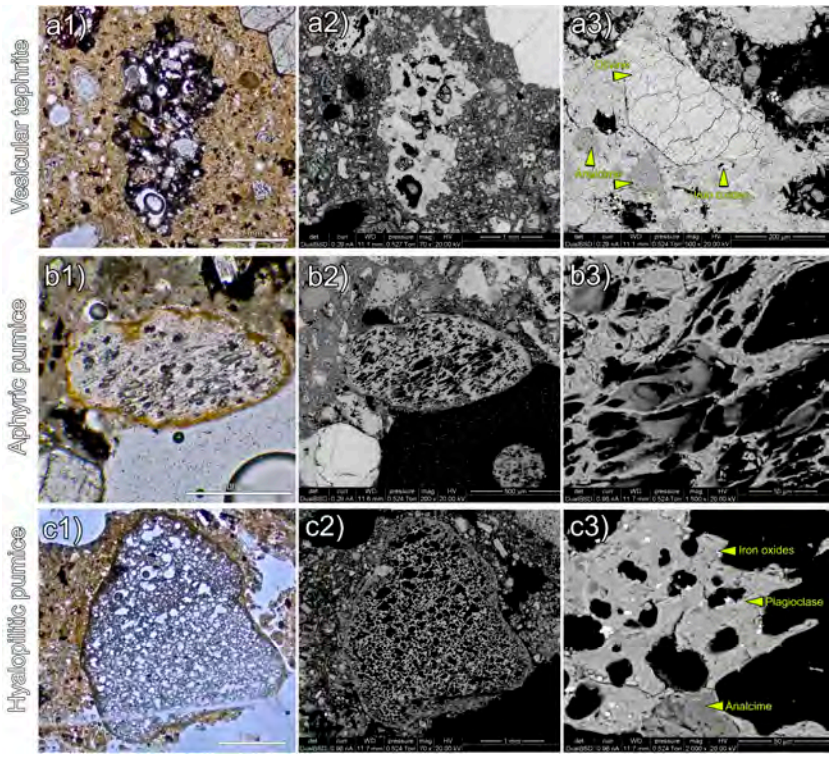

Figure 8. OM-TL (parallel nicols) and SEM (backscattered electrons) acquisition of representative volcanic clasts included in mortars. (**a1**–**a3**) vesicular tephrite; (**b1**–**b3**) aphyric pumice; (**c1**–**c3**) hyalopilitic pumice.

Finally, although sample M332 is probabilistically associated by DA to group 2b or group 3b (with nearly equal likelihood), petrographic analysis suggests it does not exhibit significant differences from the group 2b samples (Figure 6d). Thus, it is more plausibly associated with group 2b, aligning with the observations from the PCA distributions. The mortar features observed via OM coupled with SEM-EDS support the PCA distribution of samples according to their QPA-XRPD profiles.

In conclusion, samples from group 3a are positively correlated with trend vectors for plagioclase, hematite, clinopyroxene, and olivine, indicative of the common mineralizations detected in the high tephritic/cineritic fraction present in these composites. In contrast, group 2a samples exhibit an inverse correlation in respect to the mineralogical phases that characterize group 3a mortars. In fact, group 2a mortars feature positive correlations of amorphous fraction and biotite content, which reflects the elevated presence of aphyric pumice in the mortars of these composites. Intermediate correlations are observed in group 2b samples, which show a high concentration of analcime, attributable to the analcimized leucites found in both vesicular tephrites and certain pumices. These mineral phase vectors, in turn, are entirely counter-correlated with samples from modern restorations, distinguished by positive correlations with calcite content (indicative of lime-rich mortars), quartz (different source of certain aggregates), and leucite [10]. In particular, the high

leucite content in the group 1 mortars is likely associated with the presence of pumice fragments enriched with leucite, characterized by abundant mineralizations within the volcanic glass unaffected by analcimization, as detected in modern restoration sample M259 analyzed in [10] (Figure 10).

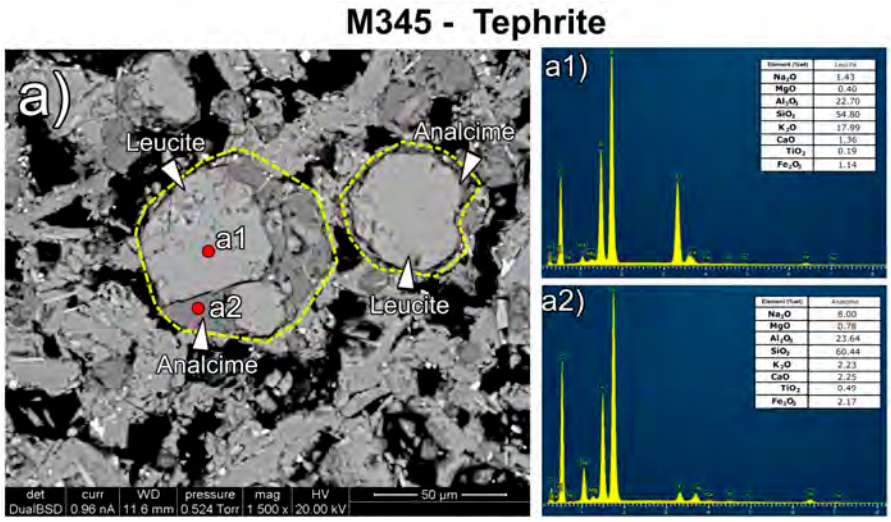

Figure 9. Leucite mineralization in a tephrite included in sample M345. (**a**) SEM image (backscattered electron) of the leucite mineral with clear analcimization rims; (**a1**,**a2**) EDS microanalyses in two points of the analcimized leucite.

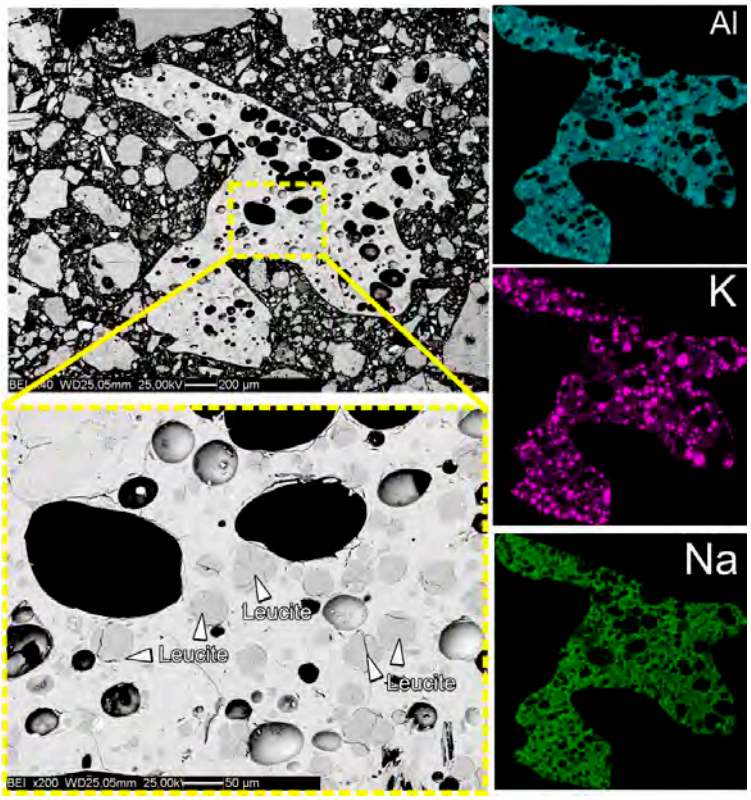

Figure 10. SEM-EDS analysis of a pumice clast embedded in modern restoration mortar M259 (as analyzed in [10]). BEI micrographs reveal the presence of fresh leucite mineralization within the volcanic glass, whereas analcime rims are not detected. EDS maps confirm this observation, showing distinct K-enriched and mildly Al-enriched regions corresponding to the leucite minerals, with no detectable Na-enriched areas—further evidence of the absence of analcimization processes.

6. Discussion

6.1. Sequencing Building Interventions

The analyses of the 2022 mortars allowed the sampled structures to be attributed with certainty to a specific building phase based on the characteristics of the mortar employed (Figure 11). In some cases, the analytical results confirmed the hypotheses already proposed on an archaeological–stratigraphic basis. In other instances, the analysis resolved uncertainties regarding the attribution of certain structures to specific building phases. Notably, the absence of differences between the mortars used in the foundations and those in the elevations clarified that certain structures (USM 80, 300, and 301) were not constructed atop older walls but were entirely built within the same phase (phase III) from the foundation upward. This insight enabled a more accurate interpretation of the building's architectural evolution and construction processes.

The analysis also provided critical insights for refining the sequence of construction activities within the complex. Notably, the classification of sample M338 within group 2b revealed an important revision of prior assumptions [10]. In fact, it demonstrated that mortars from group 2b actually predate those of group 2a. This conclusion is supported by the fact that the sample originates from a levelled wall structure unequivocally associated with an earlier construction phase (USM 515), predating the house currently visible at civ. n. 21. Indeed, this structure is overlaid by the kitchen counter in room O, likely realized in the last phase of restoration before the 79 CE eruption (Figure 12).

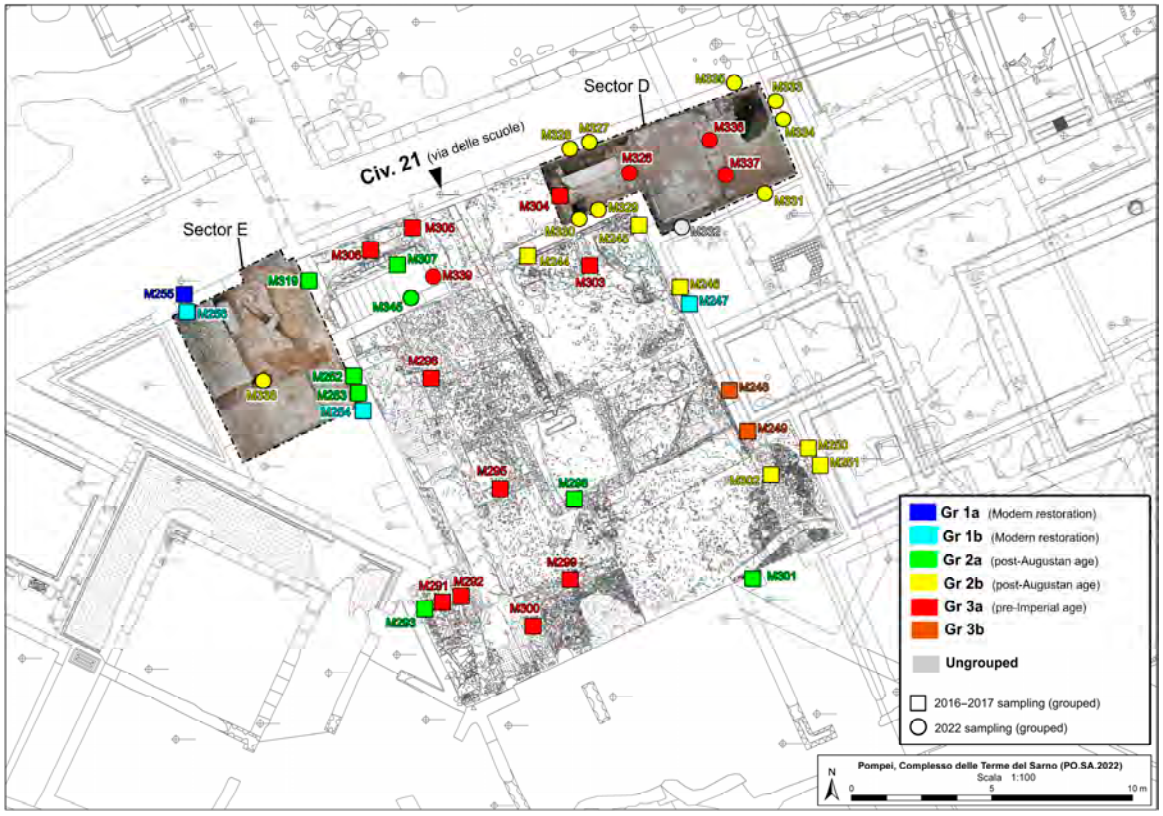

Figure 11. Samples collected from the 2022 excavation in circular labels colored according to attributed groups after the processing of analytical data.

As for the building techniques, the mortar analysis confirmed what had already been hypothesized on the basis of archaeological data, namely that in the complex there is no close relationship between construction techniques and building phases, in particular in the more recent one. In fact, even if *opus incertum* seems to predominate in phase II structures

(characterized by group 3a mortars), at least at foundation level, the same technique continued to be used in phase III structures, in which other techniques are also recognizable (*opus quasi reticulatum*, *opus vittatum mixtum*). A similar trend can also be observed with regard to the materials used in the wall structures. In phase II walls, compact and vesicular tephrite predominate (though not exclusively), while in phase III structures, a wider variety of stone materials is found (compact and vesicular tephrite, but also travertine, yellow tuff, and grey tuff), sometimes used in combination with brick.

Figure 12. The wall USM 515 overlaid by the kitchen counter in room O (sector E).

6.2. Chronology and Raw Materials

The aspects outlined above allow for an analysis of the formulation of mortars used in the building, identifying a clear evolutionary trend in the combinations of raw materials, particularly concerning the aggregates. Petrographic investigations clearly reveal a significant evolution in mortar production, especially in relation to the aggregate fraction. In the samples of group Gr 3a, attributed to phase II and associated with the earliest construction periods of the *domus* in the Sarno Bath complex, there is a predominant presence of ground vesicular tephrite, milled down into fragments or powder. These soft stones, also known as *Lava Foam* or *Lava-Schiuma* [27–29], were extensively quarried and employed in construction in Pompeii [29–32]. In the Sarno Baths, they constitute a recurrent material adopted for masonry structures [33]; in fact, this stone type was employed in the construction of phase II walls investigated along with the 2022 excavations in the civ. 21 (see Table 1). Discarded chips during the in situ cutting of these soft stones were subsequently repurposed as aggregate in the mortar production for phases I and II. According to the TAS diagram (Figure 13a), these clasts exhibit a chemical composition ranging from basaltic trachyandesite (approaching shoshonite) to tephriphonolite, aligning perfectly with the chemical range of Somma–Vesuvius lavas [34,35] (for the results of the SEM-EDS analyses on volcanic aggregates, see Supplementary Materials S3).

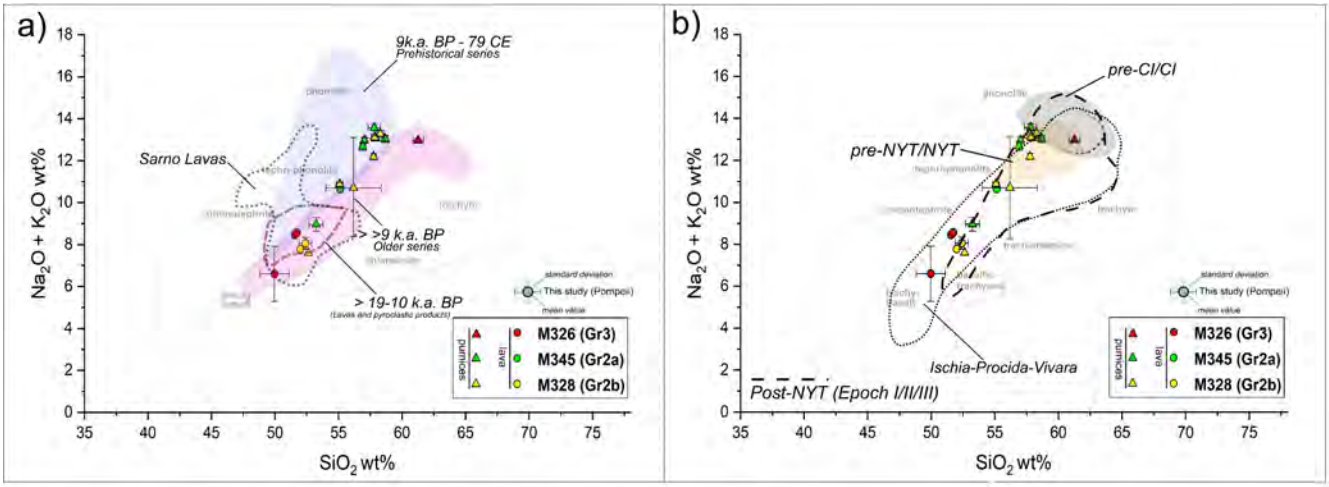

Figure 13. TAS scatterplots of pumices clasts and lavas (tephrites) included in samples M326 (Gr 3a), M345 (Gr 2a), and M328 (Gr 2b), respectively, overlapped to the geochemical intervals of compatible volcanic products of the Neapolitan district: (**a**) three primary eruptive facies of Somma–Vesuvius (reference from [22] and related sources; lava geochemical intervals are modified from [30]); (**b**) main eruptive events of the Phlegraean Fields, comprising pre-Campanian and Campanian Ignimbrite (pre-CI/CI), pre-Neapolitan and Neapolitan Yellow Tuff (pre-NYT/NYT), post-NYT, and Phlegraean-correlated volcanoes of Ischia and Procida–Vivara (reference from [22] and related sources).

In the mortars of group Gr 2b, we detected a significant increase in pumice grains, which become predominant in group Gr 2a, although vesicular tephrite lavas remain present to some extent. Moreover, silica-undersaturated pumice clasts, which range in composition from tephriphonolite to basaltic trachyandesite, are less common. In contrast, most of the juveniles, and in particular the aphyric clasts, primarily exhibit a phonolitic chemical composition. This geochemical composition overlaps with the main Phlegraean volcanic products [36,37] (Figure 13b) as well as the Somma–Vesuvius older (>9 k.a. BP) and prehistorical (9 k.a. BP—79 CE) Plinian and sub-Plinian explosive series [38,39] (Figure 13a). Consistent with the findings of [8] regarding the clasts present in Pompeian mortars from the Samnite period, our analysis of the Gr 3a mortars, associated with pre-Imperial construction phases, similarly outlines the absence of pumices with phonolitic compositions. Moreover, it is noteworthy that such chemical compositions are often identified in mortars through the analysis of pumices serving as pozzolanic aggregates, where these clasts are associated with Phlegraean eruptions [16,22,40], particularly those occurring after the Neapolitan Yellow Tuff event (post-NYT eruptions). This aspect aligns well with the increasing use of yellow tuff in masonry, likely linked to Phlegraean volcanic activity [36,37], particularly during the pre- and post-earthquake renovations of 62/63 CE. The first evidence of its use extends back to the late Republican period and continues to expand into later decades [32,41,42]. The increasing use of yellow tuff as masonry material in the construction and reconstruction activities of the Imperial period in Pompeii could therefore be associated with the growing presence of non-lithified pyroclastic debris, such as pumice and aphyric shards, which were used as pozzolanic aggregates in mortars and likely sourced predominantly from Phlegraean-related deposits.

7. Conclusive Remarks

The multi-analytical protocol we adopted, primarily based on the processing of mineralogical QPA-XRPD data using multivariate statistical analysis techniques, proved highly effective in distinguishing construction phases and identifying raw materials used in the Sarno Bath complex. This effectiveness is contingent on the availability of a comprehensive reference dataset of samples associated with well-defined phases. The dataset must encom-

pass all potential phases and subphases to ensure reliable classification of unknown samples. The method we adopted acts like a machine-learning tool, efficiently assigning samples to groups based on a well-classified training dataset. This semi-automated protocol is both cost effective and time efficient, addressing group classification challenges with high confidence by maximizing the use of the mineralogical characteristics of the samples. Ambiguous cases, identified by low probabilistic attribution through discriminant analysis, are flagged for further verification using complementary techniques such as optical microscopy and SEM-EDS. Cross-validation of data and comparison with archaeological results has demonstrated the method's effectiveness. Following this data processing, the samples still remaining uncertain are limited to a few instances (e.g., M332). In such cases, it may be necessary to employ other advanced techniques (e.g., XRF on bulk mortars, or FT-IR) to more confidently define their group affiliations or confirm their status as outliers.

In conclusion, this method can streamline workflows and reduce subjective and speculative interpretations and assumption. Therefore, it could be effectively applied to the study of other ancient buildings with long construction histories, not limited to Vesuvian sites. However, it is crucial to first establish a comprehensive reference dataset that captures the variability of ancient and modern mortars with a well-defined chronology. Such a dataset can then be used to attribute other structures of uncertain chronology to specific construction or restoration episodes.

Finally, this analytical protocol can significantly aid structural investigations for diagnostic purposes and maintenance or restoration of buildings by distinguishing sectors constructed at different times, which therefore may present diverse conservation risks. From an archaeological perspective, it provides a cost-effective alternative to the extensive and time-consuming stratigraphic excavation traditionally needed to establish the chronology of structures based on associated artifact assemblages and absolute dating methods (i.e., ^{14}C), or alternatively serves as an efficient pre-screening tool for guiding targeted and spatially limited stratigraphic investigations.

Supplementary Materials: The following supporting information can be downloaded at: https://www.mdpi.com/article/10.3390/heritage8020051/s1, S1: Instrumental equipment and standards; S2: Results of the QPA-XRPD analyses; S3: Results of the SEM-EDS analyses on volcanic aggregates.

Author Contributions: Conceptualization S.D.; methodology, S.D., M.S.; validation, S.D., C.P.; formal analysis, S.D.; investigation, S.D., C.P.; resources, M.S.B.; data curation, S.D., C.P.; writing—original draft preparation, S.D. (Sections 1, 2, 4, 5, 6.2, 6.3, 7), C.P. (4, 6.1), M.S.B. (3); writing—review and editing, S.D., C.P., M.S., M.S.B.; visualization, S.D., C.P.; funding acquisition, S.D., M.S.B. All authors have read and agreed to the published version of the manuscript.

Funding: This research was funded by the project "Trade and use of volcanic pozzolans in the Roman world. A natural material for the production of eco-sustainable concrete of antiquity" (Principal investigator: Simone Dilaria, BIRD 2023 of the Department of Cultural Heritage of the University of Padua, project code BIRD230232/23). The research infrastructures were implemented and funded within the scopes of the University of Padua under the World Class Research Infrastructures (WCRI) program—SYCURI (Synergic Strategies for Culture Heritage at Risk).

Data Availability Statement: The data presented in this study are available on request from the corresponding authors.

Acknowledgments: The complex has been the subject of study by the University of Padua since 2016 by virtue of an initial agreement signed initially with the then Special Superintendence of Pompeii (prot. STPD11B3LB), then with the Archaeological Park of Pompeii (Rep. no. 71/2020, prot. no. 1310 of 4 August 2020). We would like to thank M. Osanna, G. Zuchtriegel, and the successive officials of *Regio* VIII (S. Masseroli, L. D'Esposito, F. Muscolino and the current G. Scarpati) for their helpfulness and fruitful cooperation.

Conflicts of Interest: The authors declare no conflicts of interest.

References

1. Piovesan, R.; Curti, E.; Grifa, C.; Maritan, L.; Mazzoli, C. Ancient plaster technology: Petrographic and microstratigraphic analysis of plaster-based building materials from the Temple of Venus, Pompeii. In *Interpreting Silent Artefacts: Petrographic Approaches to Archaeological Ceramics*; Quinn, P.S., Ed.; Archaeopress: Oxford, UK, 2009; pp. 65–79.
2. Freccero, A. *Pompeian Plasters, Insula I 9 and Forum*; The Swedish Institute in Rome. Projects and Seminars 5:1; Swedish Institute in Rome Publication: Rome, Italy, 2005.
3. Bonazzi, A.; Santoro, S.; Mastrobattista, E. Caratterizzazione archeometrica delle malte e degli intonaci dell'Insula del Centenario. In *Pompei. Insula del Centenario (IX, 8) I. Indagini Diagnostiche Geofisiche e Analisi Archeometriche*; Santoro, S., Ed.; Studi e Scavi. Nuova Serie 16; Ante Quem: Bologna, Italy, 2007; pp. 93–128.
4. Demauro, T. Lo studio delle malte. Strumento di verifica. In *Restauri a Pompei (1748–1860)*; Demauro, T., Ed.; Studi e Ricerche del Parco Archeologico di Pompei 44; «L'Erma» di Bretschneider: Roma, Italy, 2020; pp. 143–161.
5. Miriello, D.; Barca, D.; Bloise, A.; Ciarallo, A.; Crisci, G.M.; De Rose, T.; Gattuso, C.; Gazineo, F.; La Russa, M.F. Characterisation of archaeological mortars from Pompeii (Campania, Italy) and identification of construction phases by compositional data analysis. *J. Archaeol. Sci.* **2010**, *37*, 2207–2223. [CrossRef]
6. Miriello, D.; Bloise, A.; Crisci, G.M.; De Luca, R.; De Nigris, B.; Martellone, A.; Osanna, M.; Pace, R.; Pecci, A.; Ruggieri, N. New compositional data on ancient mortars and plasters from Pompeii (Campania—Southern Italy): Archaeometric results and considerations about their time evolution. *Mater. Charact.* **2018**, *146*, 189–203. [CrossRef]
7. De Luca, R.; Miriello, D.; Pecci, A.; Domínguez-Bella, S.; Bernal-Casasola, D.; Cottica, D.; Bloise, A.; Crisci, G.M. Archaeometric Study of Mortars from the Garum Shop at Pompeii, Campania, Italy. *Geoarchaeology* **2015**, *30*, 330–351. [CrossRef]
8. Franceschini, M.M.N.; Casa, G.; Calandra, S.; Ismaelli, T.; Grifa, C.; Mercurio, M.; Amoretti, V.; Zuchtriegel, G.; Cantisani, E. Raw materials and building technologies in the public buildings of Pompeii after the earthquake of 62/63 CE: A diachronic analysis of mortars. *Case Stud. Constr. Mater.* **2024**, *21*, e03943. [CrossRef]
9. Secco, M.; Previato, C.; Addis, A.; Zago, G.; Kamsteeg, A.; Dilaria, S.; Canovaro, C.; Artioli, G.; Bonetto, J. Mineralogical clustering of the structural mortars from the Sarno Baths, Pompeii: A tool to interpret construction techniques and relative chronologies. *J. Cult. Herit.* **2019**, *40*, 265–273. [CrossRef]
10. Dilaria, S.; Previato, C.; Secco, M.; Busana, M.S.; Bonetto, J.; Cappellato, J.; Ricci, G.; Artioli, G.; Tan, P. Phasing the history of ancient buildings through PCA on mortars' mineralogical profiles: The example of the Sarno Baths (Pompeii). *Archaeometry* **2022**, *64*, 866–882. [CrossRef]
11. Boedeker, P.; Kearns, N.T. Linear Discriminant Analysis for Prediction of Group Membership: A User-Friendly Primer. *Adv. Methods Pract. Psychol. Sci.* **2019**, *2*, 250–263. [CrossRef]
12. Montana, G.; Cau Ontiveros, M.Á.; Polito, A.M.; Azzaro, E. Characterisation of clayey raw materials for ceramic manufacture in ancient Sicily. *Appl. Clay Sci.* **2011**, *53*, 476–488. [CrossRef]
13. Schürch, B.; Wettengl, S.; Fröhle, S.; Conard, N.; Schmidt, P. The origin of chert in the Aurignacian of Vogelherd Cave investigated by infrared spectroscopy. *PLoS ONE* **2022**, *17*, e0272988. [CrossRef]
14. Prochaska, W. The use of geochemical methods to pinpoint the origin of ancient white marbles. *Mineral. Petrol.* **2023**, *117*, 401–409. [CrossRef]
15. Dilaria, S.; Bonetto, J.; Germinario, L.; Previato, C.; Girotto, C.; Mazzoli, C. The stone artifacts of the National Archaeological Museum of Adria (Rovigo, Italy): A noteworthy example of heterogeneity. *Archaeol. Anthr. Sci.* **2024**, *16*, 14. [CrossRef]
16. Dilaria, S.; Ricci, G.; Secco, M.; Beltrame, C.; Costa, E.; Giovanardi, T.; Bonetto, J.; Artioli, G. Vitruvian binders in Venice: First evidence of Phlegraean pozzolans in an underwater Roman construction in the Venice Lagoon. *PLoS ONE* **2024**, *19*, e0313917. [CrossRef] [PubMed]
17. Artioli, G.; Ghedini, E.F.; Modena, C.; Bonetto, J.; Busana, M.S. Foreword: The MACH Project and the case study of the Sarno Baths in Pompeii. *J. Cult. Herit.* **2019**, *40*, 228. [CrossRef]
18. Bernardi, L.; Busana, M.S. The Sarno Baths in Pompeii: Context and state of the art. *J. Cult. Herit.* **2019**, *40*, 231–239. [CrossRef]
19. Busana, M.S.; Andreatta, C. Abitare a Pompei 'Vista Mare': Il Caso del Complesso delle Terme del Sarno (VIII 2, 17–23). *Atlante Temat. Topogr. Antica 36* **2019**, *in press*.
20. Rietveld, H.M. Line Profiles of Neutron Powder-diffraction Peaks for Structure Refinement. *Acta Crystallogr.* **1967**, *22*, 151–152. [CrossRef]
21. Dollase, W. Correction of Intensities for Preferred Orientation in Powder Diffractometry: Application of the March Model. *J. Appl. Crystallogr.* **1986**, *19*, 267–272. [CrossRef]
22. Dilaria, S.; Ghiotto, A.R.; Secco, M.; Furlan, G.; Giovanardi, T.; Zorzi, F.; Bonetto, J. Early exploitation of Neapolitan pozzolan (pulvis puteolana) in the Roman theatre of Aquileia, Northern Italy. *Sci. Rep.* **2023**, *13*, 4110. [CrossRef]
23. Melander, J.M.; Lauersdorf, L.R. *Masonry: Design and Construction, Problems and Repair*; ASTM: Philadelphia, PA, USA, 1993.
24. Leone, G.; De Vita, A.; Magnani, A.; Rossi, C. Characterization of archaeological mortars from Herculaneum. *Thermochim. Acta* **2016**, *624*, 86–94. [CrossRef]

25. Fahmy, A.; Molina-Piernas, E.; Martínez-López, J.; Domínguez-Bella, S. Salt weathering impact on Nero/Ramses II Temple at El-Ashmonein archaeological site (Hermopolis Magna), Egypt. *Herit. Sci.* **2022**, *10*, 125. [CrossRef]
26. Giampaolo, C.; Godano, R.F.; Di Sabatino, B.; Barrese, E. The alteration of leucite-bearing rocks: A possible mechanism. *Eur. J. Miner.* **1997**, *9*, 1293–1310. [CrossRef]
27. Cinque, A.; Irollo, G. Il "vulcano di Pompei": Nuovi dati geomorfologici e stratigrafici. *Quat. Ital. J. Quat. Sci.* **2004**, *17*, 101–116.
28. Di Girolamo, P. Un esempio di lava schiuma (foam lava) in Campania (Lava schiuma di Pompei Scavi). *Rend. Accad. Sci. Fis. Mat. (Sez. Soc. R. Napoli) Napoli* **1968**, *4*, 4–12.
29. Frizot, M. Caracterization des materiaux de construction de Pompei. In *Dégradation et Restauration de l'architecture Pompéienne*; Adam, J.-P., Frizot, M., Eds.; Éditions du Centre National de la Recherche Scientifique: Paris, France, 1983; pp. 32–41.
30. Kastenmeier, P.; Di Maio, G.; Balassone, G.; Boni, M.; Joachimski, M.; Mondillo, N. The source of stone building materials from the Pompeii archaeological area and its surroundings. *Period. Mineral.* **2010**, *79*, 39–58. [CrossRef]
31. Dessales, H. Les savoir-faire des maçons romains, entre connaissance technique et disponibilité des matériaux. Le cas pompéien. In *Les Savoirs Professionnels des Gens de Métier. Études Sur le Monde du Travail Dans les Sociétés Urbaines de l'empire Romain*; Monteix, N., Tran, N., Eds.; Centre Jean Bérard: Napoli, Italy, 2011; pp. 41–63.
32. Covolan, M. *Tufo Gallo: Cantieri di Costruzione ed Economia del Tufo a Pompei*; Costruire nel Mondo Antico 6; Quasar: Roma, Italy, 2023.
33. Piovesan, R.; Maritan, L.; Meneghin, G.; Previato, C.; Baklouti, S.; Sassi, R.; Mazzoli, C. Stones of the façade of the Sarno Baths, Pompeii: A mindful construction choice. *J. Cult. Herit.* **2019**, *40*, 255–264. [CrossRef]
34. Santacroce, R.; Cioni, R.; Marianelli, P.; Sbrana, A. Understanding Vesuvius and preparing for its next eruption. In *Cultural Responses to the Volcanic Landscape: The Mediterranean and Beyond*; Balmuth, M.S., Chester, D.K., Johnston, P.A., Eds.; Colloquia and Conference Papers 8; Archaeological Institute of America: Boston, MA, USA, 2007; pp. 27–55.
35. Guarino, V.; Solone, R.; Casalini, M.; Franciosi, L.; Dallai, L.; Morra, V.; Conticelli, S.; Melluso, L. The geochemistry of leucite-bearing lavas from early stages of the Somma-Vesuvius volcanic complex: Feeder systems and mantle enrichment processes in the Neapolitan district of the Roman Magmatic Province. *Geochemistry* **2024**, *84*, 126076. [CrossRef]
36. Peccerillo, A. Campania volcanoes: Petrology, geochemistry, and geodynamic significance. In *Vesuvius, Campi Flegrei, and Campanian Volcanism*; De Vivo, B., Belkin, H.E., Rolandi, G., Eds.; Elsevier: Amsterdam, The Netherlands, 2020; pp. 79–120. [CrossRef]
37. Morra, V.; Calcaterra, D.; Cappelletti, P.; Colella, A.; Fedele, L.; de Gennaro, R.; Langella, A.; de Gennaro, M.; Mercurio, M. Urban geology: Relationships between geological setting and architectural heritage of the Neapolitan area. *J. Virtual Explor.* **2010**, *36*, 26. [CrossRef]
38. Santacroce, R.; Cioni, R.; Marianelli, P.; Sbrana, A.; Sulpizio, R.; Zanchetta, G.; Donahue, D.J.; Joron, J.L. Age and whole rock–glass compositions of proximal pyroclastics from the major explosive eruptions of Somma-Vesuvius: A review as a tool for distal tephrostratigraphy. *J. Volcanol. Geotherm. Res.* **2008**, *177*, 1–18. [CrossRef]
39. Melluso, L.; Scarpati, C.; Zanetti, A.; Sparice, D.; de' Gennaro, R. The petrogenesis of chemically zoned, phonolitic, Plinian and sub-Plinian eruptions of Somma-Vesuvius, Italy: Role of accessory phase removal, independently filled magma reservoirs with time, and transition from slightly to highly silica undersaturated magmatic series in an ultrapotassic stratovolcano. *Lithos* **2022**, *430–431*, 106854. [CrossRef]
40. Rispoli, C.; De Bonis, A.; Esposito, R.; Sossio, F.G.; Langella, A.; Mercurio, M.; Morra, V.; Cappelletti, P. Unveiling the secrets of Roman craftsmanship: Mortars from Piscina Mirabilis (Campi Flegrei, Italy). *Archaeol. Anthr. Sci.* **2020**, *12*, 8. [CrossRef]
41. Dessales, H. *The Villa of Diomedes: The Making of a Roman Villa in Pompeii*; HERMANN: Paris, France, 2020.
42. Dessales, H. Les constructions en tuf jaune dans la Campanie romaine: Usages et modalités d'entretien. In *Sarta Tecta. De l'entretien à la Conservation des Édifices, Antiquité, Moyen Âge, Début de la Période Moderne*; Davoine, C., L'Héritier, M., Péron d'Harcourt, A., Eds.; BiAMA 26; Presses Universitaires de Provence: Aix-en-Provence, France, 2019; pp. 59–69.